Controlling Ionic Conductivity in Organometallic Ionic Liquids through Light-Induced Coordination Polymer Formation and Thermal Reversion

Mochida, Tomoyuki ; Shimada, Masato ; Inoue, Ryota ; Sumitani, Ryo ; Funasako, Yusuke ; Yamada, Hiroki

(Citation)
The Journal of Physical Chemistry B,128(25):6207-6216

(Issue Date)
2024-06-27

(Resource Type)
journal article

(Version)
Accepted Manuscript

Controlling Ionic Conductivity in Organometallic Ionic Liquids through Light-Induced Coordination Polymer Formation and Thermal Reversion

Tomoyuki Mochida,[a,b] Masato Shimada,[a] Ryota Inoue,[a] Ryo Sumitani,[a] Yusuke Funasako,[c] and Hiroki Yamada[d]*

[a]Department of Chemistry, Graduate School of Science, Kobe University, Rokkodai, Nada, Kobe, Hyogo 657-8501, Japan. E-mail: tmochida@platinum.kobe-u.ac.jp

[b]Research Center for Membrane and Film Technology, Kobe University, Rokkodai, Nada, Kobe, Hyogo 657-8501, Japan

[c]Department of Applied Chemistry and Biochemistry, National Institute of Technology, Wakayama College, 77 Noshima, Nada, Gobo, Wakayama, Japan

[d]Japan Synchrotron Radiation Research Institute (JASRI), Kouto 1-1-1, Sayo-cho, Sayo-gun, Hyogo 679-5198, Japan

KEYWORDS: ionic liquids, coordination polymers, ionic conductivity, photochemical reaction, Ru complexes

ABSTRACT: Owing to their high ionic conductivity and negligible vapor pressure, ionic liquids (ILs) find applications in various electronic devices. However, fabricating IL-based photocontrollable devices remains a challenge. In this study, we developed organometallic ILs with reversible light- and heat-controlled ionic conductivities for potential use in tunable devices. The physical properties and stimulus responses of ILs containing a cationic sandwich Ru complex with two coordinating substituents were investigated. UV photoirradiation of these ILs

triggered cation photodissociation, resulting in their transformation into viscoelastic coordination polymers wherein the coordinating substituents bridged the Ru centers. Owing to the anion coordination, salts with coordinating anions such as $CF_3SO_2NCN^-$, $B(CN)_4^-$, and $BF_2(CN)_2^-$ exhibited faster response and higher conversion than those with noncoordinating anions including $(FSO_2)_2N^-$ and $(CF_3SO_2)_2N^-$. All photoproducts reverted to their original ILs upon heating, except for the photoproduct of the $BF_2(CN)_2$ salt, which decomposed upon heating. Light- and heat-induced reversible changes occur in most cases between the high-ionic-conductive IL state and low-ionic-conductive coordination polymer state. Unlike previously reported ILs with three or one cation substituent, the current ILs exhibited both high reactivity and large ionic conductivity changes.

TOC graphics

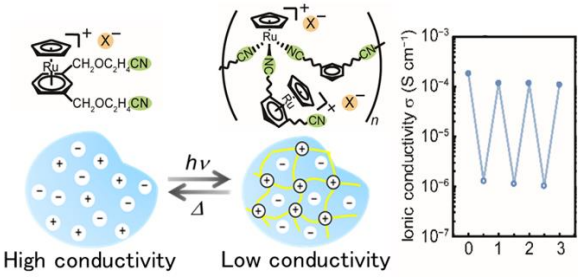

INTRODUCTION

Photocontrollable electronic devices have applications in various fields, including optical sensors, optical switches, and phototransistors. Although these devices are typically constructed from solid-state materials,[1-4] liquid materials are gaining increasing attention owing to their ease of application, film formation, self-healing properties, and suitability for flexible devices.[5-10] Ionic liquids (ILs) are particularly promising for electrochemical applications,[6-10] serving as

electrolytes[11-13] and even electronic memory devices,[14,15] because of their low volatility and high ionic conductivity. There are several ILs or ionogels that change their ionic conductivity in response to external stimuli such as carbon dioxide,[16-18] humidity,[19,20] and pH,[21] which are useful for applications in sensors. Nevertheless, only few ILs have been reported that exhibit photocontrollable ionic conduction, and their mechanism is based on photoisomerization with typically minor conductivity changes.[22-25]

In this context, we recently developed organometallic ILs[26] possessing reversible light- and heat-modulated ionic conductivities to explore photocontrollable liquid electronic materials.[27-30] Employing ILs in device applications is advantageous, as they can be used in extremely small amounts as liquid films. Photoreactive IL **3-FSA** (Figure 1a; FSA = $(FSO_2)_2N^-$), containing a cationic Ru sandwich complex, undergoes cation photodissociation upon UV photoirradiation, and the reaction yields an amorphous coordination polymer where cyano groups bridge Ru ions, thereby reducing the ionic conductivity.[27,30] Heating reverses the photoproduct to its original IL, with the ionic conductivity exhibiting a reversible change. However, a prolonged photoreaction time (~300 min) renders this IL impractical. In contrast, **1-FSA**, bearing a single substituent (Figure 1b), is trimerized upon UV photoirradiation and converted into a high-viscosity liquid, and its photoreaction time is much faster (~10 min).[27] However, it exhibits smaller changes in ionic conductivity, and the reversible reaction occurs easily, even at ambient temperature.

The present study introduces Ru-containing organometallic ILs **2-X** possessing two cyanoalkyl substituents (Figure 2; X = anion). In addition, **4-FSA** was synthesized to examine the effect of an electron-donating substituent on the photoreactivity. This study revealed that the reduced number and shorter length of substituents in **2-X** relative to **3-FSA** led to the former's lower melting point and reduced viscosity, thereby enabling fast photoresponse and large ionic conductivity changes. In particular, we examined the effect of incorporating noncoordinating

anion (FSA and Tf_2N) and coordinating anion (TfNCN, $B(CN)_4$, and $BF_2(CN)_2$) on the photoreactivity. In **2-X**, when noncoordinating anions were incorporated, photodissociation of the 2/3 of cations resulted in all cyano groups coordinating with the Ru ion, preventing further photoreaction owing to the saturation of the three cyano groups on the Ru ion (Figure 3a). However, **2-X** exhibited a faster reaction and higher conversion resulting from additional anion coordination when incorporated with coordinating anions (Figure 3b). These ILs mostly exhibited reversible changes in ionic conductivity upon exposure to light and heat, and the reactivity and reversibility were anion dependent. Furthermore, structural changes of the ILs before and after photoirradiation were investigated using the X-ray pair distribution function (PDF) analysis.

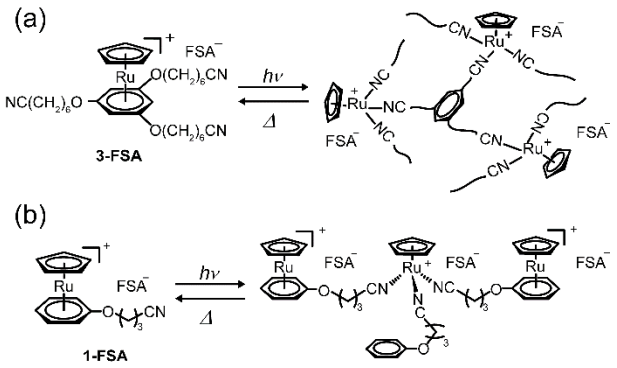

Figure 1. Photoreaction and thermal reaction of the photoreactive Ru-containing ILs (a) **3-FSA** and (b) **1-FSA**. In Figure (a), alkyloxy substituents are represented using wavy lines.

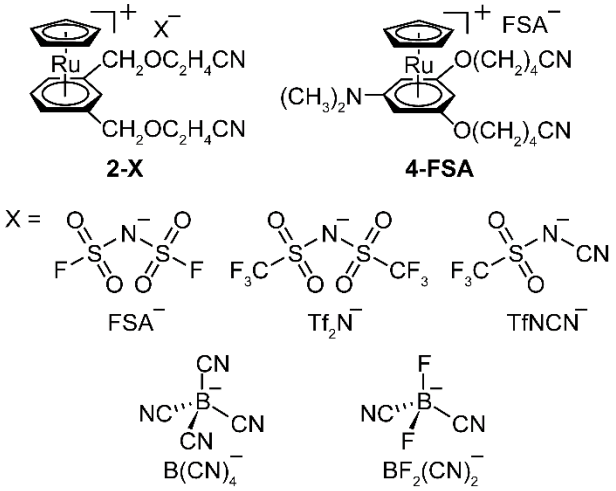

Figure 2. Structural formulas of **2-X** (X = FSA, Tf_2N, TfNCN, $B(CN)_4$, and BF_2CN_2) and **4-FSA**.

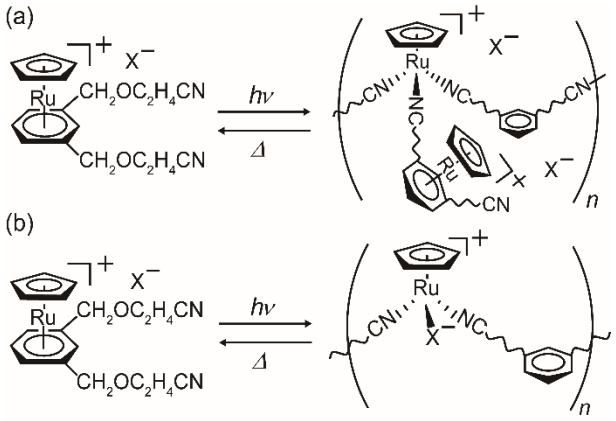

Figure 3. Photoreactions anticipated in ILs with (a) noncoordinating anions and (b) coordinating anions. The substituents are represented by wavy lines.

METHODS

General Procedures. K[TfNCN],[31] K[$BF_2(CN)_2$],[32] and 5-dimethylaniline resorcinol[33] were prepared following methods reported previously. ^1H and ^{19}F NMR, FT-IR, and UV–Vis spectra were recorded using a Bruker Avance 400 spectrometer, Thermo Nicolet iS5 or Jasco FT/IR-4700 with a microscope attachment, and a JASCO V–570 UV/VIS/NIR spectrophotometer,

respectively. The samples were carefully vacuum dried prior to physical measurements. Differential scanning calorimetry (DSC) was performed using a TA Instrument Q100 differential scanning calorimeter at a scan rate of 10 K min^{-1}. Viscosity and dynamic viscoelasticity were measured using a TA Instruments DHR-1 with ϕ8 mm parallel plates. A Hamamatsu LC-L1V3 Lightningcure UV-LED (365 nm, 650 mW cm^{-2}) was used for photoirradiation, during which ILs were sandwiched between quartz plates (sample thickness ~10 μm) and placed on a cooling plate (10°C). Ionic conductivity was measured using a Solartron 1260 impedance analyzer. Each sample was sandwiched between gold interdigitated electrodes (gap dimension: 200 μm, Metrohm) and a quartz glass plate and further sealed with epoxy resin for conductivity measurements, where the sample thickness was larger than 10 μm. For calibrating ionic conductivity, the sample thickness was set to 89 μm.

PDF analysis. High-energy X-ray total scattering measurements were performed at the BL04B2 high-energy XRD beamline (SPring-8, Japan) for calculating PDF.[34] IL was packed into a glass capillary, and scattering patterns were measured at room temperature using the CdTe two-dimensional detectors. The energy of the incident X-rays was 112.8 keV, and the maximum Q ($Q = 4\pi \sin\theta/\lambda$), Q_{max}, was 23 $Å^{-1}$.

Synthesis of 1,3-Bis(4-cyanobutyloxy)benezene (L^1). A mixture of 1,3-bis(bromomethyl)benzene (550 mg, 2.1 mmol), 3-hydroxypropionitrile (364 mg, 5.0 mmol), and diisopropylethylamine (727 mg, 5.6 mmol) was refluxed for 5 h under a nitrogen atmosphere. After cooling the mixture to room temperature, ethyl acetate (5 mL) and a 10% sodium hydrogen sulfate aqueous solution (7 mL) were added and stirred for 10 min. The solution was extracted five times with ethyl acetate (5 mL), and the organic layer was dried over anhydrous magnesium sulfate. A yellow liquid was obtained after solvent evaporation, which was then sonicated after

adding hexane, and the hexane layer was removed. This procedure was repeated 10 times. The crude product was purified using column chromatography (alumina, eluent: EtOAc:hexane = 1:4–1:0; R_f = 0.4) to give a pale-yellow liquid, which was dried under vacuum at 70°C for 2 h (166 mg, 34% yield). ^{1}H NMR (400 MHz, $CDCl_3$): δ = 2.64 (t, 4H, C*H*$_2$CN, J = 6.02 Hz), 3.70 (t, 4H, OC*H*$_2$CH$_2$CN, J = 6.03 Hz), 4.59 (s, 4H, ArC*H*$_2$O), 7.26–7.39 (m, 4H, Ar-*H*$_4$).

Synthesis of 3,5-bis(4-cyanobutyloxy)-*N*,*N*-dimethylaniline (L^2). An acetonitrile solution (50 mL) of 5-dimethylaniline resorcinol (700 mg, 4.57 mmol), 5-bromopentanenitrile (1.85 g, 11.4 mmol), K_2CO_3 (5.50 g, 39.8 mmol), and tetrabutylammonium chloride (70.0 mg, 0.252 mmol) was refluxed for 24 h. After cooling to room temperature, the solution was filtered, and the solvent was evaporated. The crude product was purified using column chromatography (silica gel, eluent: CH_2Cl_2) and further purified by recrystallization from MeOH. The product was obtained as pale orange platelet crystals (0.82 g, 57% yield). ^{1}H NMR (400 MHz, $CDCl_3$, TMS): δ = 1.92 (m, 8H), 2.44 (t, J = 6.8 Hz, 4H), 2.92 (s, 6H), 3.98 (t, J = 5.4 Hz, 4H), 5.85–5.88 (m, 3H).

Synthesis of [CpRu(L^1)]X (2-X; X = FSA, Tf_2N, TfNCN, $B(CN)_4$, $BF_2(CN)_2$, and Cp = C_5H_5). An acetonitrile solution (4.5 mL) of [CpRu(CH_3CN)$_3$]PF_6 (208 mg, 0.584 mmol) and L^1 (147 mg, 0.602 mmol) was refluxed for 17 h under nitrogen atmosphere. The solvent was then evaporated, and the residue was heated under vacuum at 120°C for 30 min. The crude product was dissolved in chloroform and passed through a short column of alumina (eluent $CHCl_3$:CH_3CN = 1:0–0:1). A solution of the product in acetonitrile was treated with activated carbon, filtered, and the solvent evaporated. The PF_6 salt was obtained as a pale-yellow liquid, which was dried under vacuum 70°C for 2 h (212 mg, 65% yield). ^{1}H NMR (400 MHz, CD_3CN): δ = 2.75 (t, 4H, CH_2C*H*$_2$CN, J = 5.89 Hz), 3.81 (t, 4H, C*H*$_2$CH$_2$CN, J = 5.89 Hz), 4.42 (s, 4H,

C*H*$_2$OC$_2$H$_4$CN, *J* = 5.23 Hz), 5.38 (s, 5H, Cp-*H*$_5$), 6.12–6.36 (m, 4H, Ar-*H*$_4$). Anal. Calcd. for $C_{19}H_{21}F_6N_2O_2PRu$: C, 41.09; H, 3.81; N, 5.04. Found: C, 41.23; H, 3.96; N, 4.92.

2-FSA was synthesized using the following procedure: K[FSA] (36 mg, 0.162 mmol) was dissolved in a small amount of water, to which an acetone solution (1 mL) of [CpRu(L^1)]PF_6 (30 mg, 0.054 mmol) was added, and the solution was stirred for 30 min. After removing acetone using an evaporator, water was added, and the mixture was extracted five times with dichloromethane. The organic layer was combined, washed twice with water, and dried over magnesium sulfate, followed by solvent evaporation. This anion exchange procedure was repeated two more times, and the PF_6 anion disappearance (δ = −73.83, −71.92) was confirmed by the ^{19}F NMR spectrum (solvent: CD_3CN). The crude product was passed through a short column of alumina (eluent: CH_3CN). The acetonitrile solution was concentrated and treated with activated carbon, filtered, and the solvent evaporated to give a pale-yellow viscous liquid, which was dried under vacuum at 70°C for 2 h (25 mg, 80% yield). ^{1}H NMR (400 MHz, CD_3CN): δ = 2.75 (t, 4H, CH_2CH_2CN, *J* = 5.82 Hz), 3.82 (t, 4H, C*H*$_2$$CH_2CN$, *J* = 5.82 Hz), 4.43 (s, 4H, C*H*$_2$OC$_2$H$_4$CN, *J* = 5.23 Hz), 5.38 (s, 5H, Cp-*H*$_5$), 6.12–6.37 (m, 4H, Ar-*H*$_4$). Anal. Calcd. for $C_{19}H_{21}F_2N_3O_6RuS$: C 38,64, ; H, 3.58 ; N, 7.12. Found: C, 38.96; H, 3.54; N, 6.86.

2-Tf$_2$N, **2-TfNCN**, **2-B(CN)$_4$**, and **2-BF$_2$(CN)$_2$** were prepared by the same method as **2-FSA** using Li[Tf_2N], K[TfNCN], K[$B(CN)_4$], and K[$BF_2(CN)_2$], respectively, instead of K[FSA] for anion exchange. **2-Tf$_2$N** (56% yield). ^{1}H NMR (400 MHz, CD_3CN): δ = 2.76 (t, 4H, CH_2CH_2CN, *J* = 5.87 Hz), 3.80 (t, 4H, C*H*$_2$$CH_2CN$, *J* = 5.84 Hz), 4.43 (s, 4H, C*H*$_2$OC$_2$H$_4$CN, *J* = 5.23 Hz), 5.38 (s, 5H, Cp-*H*$_5$), 6.12–6.37 (m, 4H, Ar-*H*$_4$). Anal. Calcd. for $C_{21}H_{21}F_6N_3O_6RuS_2$: C, 36.52; H, 3.07; N, 6.08. Found: C, 36.35; H, 3.19; N, 6.13. **2-TfNCN** (63% yield). ^{1}H NMR (400 MHz, CD_3CN): δ = 2.76 (t, 4H, CH_2CH_2CN, *J* = 5.87 Hz), 3.81 (t, 4H, C*H*$_2$$CH_2CN$, *J* = 5.92 Hz),

4.43 (s, 4H, C*H*$_2$OC$_2$H$_4$CN), 5.38 (s, 5H, Cp-*H*$_5$), 6.12–6.38 (m, 4H, Ar-*H*$_4$). Anal. calcd. for $C_{21}H_{21}F_3N_4O_4RuS$: C, 43.22; H, 3.63; N, 9.60. Found: C, 43.21; H, 3.57; N, 9.79. **2-B(CN)$_4$** (72 % yield). ^{1}H NMR (400 MHz, CD_3CN): δ = 2.76 (t, 4H, CH$_2$C*H*$_2$CN, *J* = 5.87 Hz), 3.81 (t, 4H, C*H*$_2$CH$_2$CN, *J* = 5.92 Hz), 4.43 (s, 4H, C*H*$_2$OC$_2$H$_4$CN), 5.39 (s, 5H, Cp-*H*$_5$), 6.12–6.38 (m, 4H, Ar-*H*$_4$). Anal. calcd. for $C_{23}H_{21}BN_6O_2Ru$: C, 52.59; H, 4.03; N, 16.00. Found: C, 52.47; H, 3.91; N, 16.29. **2-BF$_2$(CN)$_2$** (77% yield). ^{1}H NMR (400 MHz, CD_3CN): δ = 2.76 (t, 4H, CH$_2$C*H*$_2$CN, *J* = 5.87 Hz), 3.81 (t, 4H, C*H*$_2$CH$_2$CN, *J* = 5.92 Hz), 4.43 (s, 4H, C*H*$_2$OC$_2$H$_4$CN), 5.38 (s, 5H, Cp-*H*$_5$), 6.12–6.38 (m, 4H, Ar-*H*$_4$). Anal. calcd. for $C_{21}H_{21}BF_2N_4O_2Ru$: C, 49.33; H, 4.14; N, 10.96. Found: C, 49.97; H, 4.36; N, 10.59.

Synthesis of [CpRu(L^2)]FSA (4-FSA). An acetonitrile solution (4.5 mL) of [CpRu(CH$_3$CN)$_3$]PF$_6$ (172 mg, 0.411 mmol) and L^2 (112 mg, 0.355 mmol) was refluxed for 19 h under a nitrogen atmosphere, after which the solvent was evaporated. The residue was vacuum dried at 120°C for 30 min, and a solution of the crude product in acetonitrile was passed through a short column of alumina (eluent CH$_3$CN:ethyl acetate = 1:2). The product was dissolved in acetonitrile, treated with activated carbon, filtered, and the solvent evaporated. The residue was vacuum dried at 70°C for 2 h to afford [CpRu(L^2)]PF$_6$ as a pale-yellow liquid (160 mg, 0.216 mmol; 53% yield). A methanol solution of NaBPh$_4$ (228.3 mg, 0.649 mmol) was added to the PF$_6$ salt, followed by 30-min stirring at 70°C. The resultant precipitate was collected by filtration, washed three times with methanol, and vacuum dried at room temperature for 2 h to give [CpRu{C$_6$H$_3$(OC$_4$H$_8$CN)$_2$NMe$_2$}]BPh$_4$ (183 mg). ^{1}H NMR (400 MHz, CD_3CN): δ = 1.15 (t, 4H, C*H*$_2$CH$_2$N(CH$_3$)$_2$, *J* = 7.04 Hz), 1.15 (t, 4H, ArOCH$_2$C*H*$_2$, *J* = 7.04 Hz), 2.50 (t, 4H, C*H*$_2$CN, *J* = 6.87 Hz), 2.85 (s, 6H, N(C*H*$_3$)$_2$), 3.87–4.01 (m, 4H, ArOC*H*$_2$), 5.18 (s, 5H, Cp-*H*$_5$), 5.63 (d, 2H, Ar-*H*$_2$), 5.97 (s, 1H, Ar-*H*$_1$), 6.86 (t, 1H, BPh$_4$-Ar-*H*$_1$), 7.02 (t, 2H, BPh$_4$-Ar-*H*$_2$), 7.26–7.32 (m,

2H, BPh_4-Ar-H_2).

Ion exchange resin Dowex 1-X8 (Cl form, 7 g) was suspended in methanol and packed in a short column, to which methanol (100 mL) was added. [CpRu(L^2)]BPh_4 (163 mg, 0.201 mmol) was dissolved in acetonitrile (1 mL), to which methanol was added (9 mL), and the solution was charged onto the column. The product was eluted using methanol (100 mL). The solvent was concentrated to approximately 10 mL, recharged to the column, and eluted with methanol. This procedure was then repeated one more time, and ^{1}H NMR spectra showed the absence of the BPh_4 anion (δ = 6.86 (t, 1H, Ar-H_1), 7.02 (t, 2H, Ar-H_2), 7.26–7.32 (m, 2H, Ar-H_2), in CD_3CN). Solvent evaporation gave [CpRu(L^2)]Cl as a pale-yellow liquid (103 mg, 99% yield).

K[FSA] (135 mg, 0.603 mmol) was dissolved in a small amount of water, after which a solution of [CpRu(L^2)]Cl (103 mg, 0.201 mmol) was added, and the mixture was stirred at room temperature for 30 min. After 5-time extraction with dichloromethane, the organic layer was washed thrice with water and dried over anhydrous magnesium sulfate. An acetonitrile solution of the crude product was then passed through a short alumina column (eluent: CH_3CN). The acetonitrile solution was concentrated, treated with activated carbon, filtered, and the solvent evaporated. The residue was vacuum dried at 70°C for 30 min to give the desired product as a pale-yellow liquid (65 mg, 50% yield). ^{1}H NMR (400 MHz, $CDCl_3$): δ = 1.789–1.877 (m, 4H, $ArOCH_2CH_2C_2H_4CN$), 1.890–1.977 (m, 4H, $ArOC_2H_4CH_2CH_2CN$), 2.48 (t, 4H, $ArOC_3H_6CH_2CN$, J = 6.85 Hz), 2.90 (s, 6H, $ArN(CH_3)_2$), 3.90–4.13 (m, 4H, $ArOCH_2C_3H_6CN$), 5.16 (s, 5H, Cp-H_5), 5.56 (d, 2H, Ar-H_2), 6.07 (s, 1H, Ar-H). Anal. Calcd. for $C_{23}H_{30}F_2N_4O_6RuS_2$: C, 41.75; H, 4.57; N, 8.47. Anal. C, 41.75; H, 4.71; N, 8.35.

RESULTS AND DISCUSSION

Physical Properties of ILs. Most of the synthesized ILs were pale-yellow liquids. Although **2-FSA**, **2-Tf$_2$N**, and **2-B(CN)$_4$** were solids with melting points near room temperature, once melted, they maintained the liquid state at room temperature. Table 1 lists the melting points (T_m) and glass transition temperatures (T_g) determined by DSC. Upon cooling, liquids of **2-X** exhibited a T_g of −42 to −68°C. When comparing ILs with different number of substituents, the T_g of FSA salts followed the order of **1-FSA** (−60°C)[27] < **2-FSA** (−58°C) < **3-FSA** (−53°C),[27] with T_g increasing with the number of substituents. **2-Tf$_2$N** (−54°C) exhibited a slightly higher T_g than **2-FSA** (−58°C). Among the ILs with coordinating anions, **2-TfNCN** (−68°C) and **2-BF$_2$(CN)$_2$** (−66°C) showed lower T_g than **2-FSA**, whereas **2-B(CN)$_4$** (−42°C) showed higher T_g, probably owing to its higher anion symmetry. **2-FSA**, **2-Tf$_2$N**, and **2-B(CN)$_4$** had T_m of 28°C, 27°C, and 52°C, respectively, with T_g/T_m (~0.71) in these ILs being consistent with the empirical relationship ($T_g/T_m = 2/3$).[35,36]

The viscosities and ionic conductivities of the studied ILs were measured at 25°C (Table 1). They were Newtonian liquids, with their viscosity in the order of **2-TfNCN** (0.46 Pa·s) < **2-FSA** (1.00 Pa·s) < **2-BF$_2$(CN)$_2$** (1.45 Pa·s) < **2-Tf$_2$N** (1.87 Pa·s) ≈ **2-B(CN)$_4$** (1.92 Pa·s), which was almost the same order as that of T_g. Their ionic conductivities were similar at 1.5–3.0 × 10^{-4} S cm^{-1}, except for **2-B(CN)$_4$** (6.6 × 10^{-5} S cm^{-1}), whose lower value probably resulted from its high viscosity. In contrast, **4-FSA** exhibited a higher T_g (−36°C) and much higher viscosity (12.9 Pa·s) than the other ILs, resulting in its low photoreactivity, as discussed below.

Table 1. Properties of ILs, including glass transition temperature (T_g), melting point (T_m), viscosity, and ionic conductivity before and after photoirradiation, measured at 25°C.

	T_g	T_m	Viscosity (Pa·s)		Ionic conductivity (S cm^{-1})	
	(°C)	(°C)	Before[b]	After	Before	After
2-FSA	−58	28	1.00	1542[c]	1.7 × 10^{-4}	7.6 × 10^{-6}

2-Tf_2N	−54	27	1.87	1566[c]	1.6×10^{-4}	1.3×10^{-6}
2-TfNCN	−68		0.46	–[e]	1.5×10^{-4}	1.0×10^{-6}
2-$B(CN)_4$	−42	52	1.92	–[e]	6.6×10^{-5}	1.1×10^{-6}
2-$BF_2(CN)_2$	−66		1.45	–[e]	3.0×10^{-4}	4.4×10^{-7}
1-FSA [a]	−60		0.92	5.2[b]	4.0×10^{-4}	3.7×10^{-5}
3-FSA [a]	−53		2.60	1.2×10^{5} [c,d]	3.1×10^{-5}	4.8×10^{-7}
4-FSA	−36		12.9	–[e]		

[a]Ref. 27. [b]Shear rate = 10^2 s^{-1}. [c]Complex viscosity at 10 rad s^{-1} (strain 0.1%). [d]Value for a sample with 55% conversion. [e]Not measured because of irreversible reaction, low reactivity, or inhomogeneity of the product.

Photochemical Reactions. Sandwiching liquid samples between quartz plates (sample thickness ~10 μm) and subsequent UV irradiation (365 nm, LED) transformed them from pale-yellow ILs to yellow viscoelastic coordination polymers. The photoreactions were less effective in bulk owing to the photoproduct's UV absorption. Figure 4 shows the reaction schemes and photographs of these samples, although the products, particularly those of **2-$BF_2(CN)_2$** and **2-$B(CN)_4$** containing a larger number of cyano groups, might actually comprise a mixture of different coordination structures. Figure 5a shows UV–Vis spectral changes, and Table 2 summarizes their photoreaction times, cation dissociation ratios, and conversions. ILs containing coordinating anions exhibited faster photoreaction and higher conversion than those containing noncoordinating anions. Heating the photoproducts triggered reversible reactions to yield the original ILs, except for **2-$BF_2(CN)_2$** undergoing decomposition. The reactions of ILs with coordinating and noncoordinating anions are discussed below.

Reactivity of ILs with Noncoordinating Anions. Figure 5b (left) shows the cation dissociation ratios of ILs containing noncoordinating anions (**2-FSA** and **2-Tf_2N**) against the photoirradiation time, along with the data for **1-FSA** and **3-FSA**,[27] as determined from the UV–Vis and ^{1}H NMR spectra (Figure S1). A total of 47% and 50% cation dissociations were achieved

for **2-FSA** and **2-Tf$_2$N** in approximately 30 and 80 min, respectively, and no further dissociation was observed with continued photoirradiation. The photoproducts were stable in air. The slower reaction of **2-Tf$_2$N** was probably due to its higher viscosity. The photoreaction times of **2-FSA** and **2-Tf$_2$N** were between those of **1-FSA** (~15 min) and **3-FSA** (~300 min). Furthermore, their conversions were 70% and 75%, respectively, which were 1.5 times the dissociation ratios because the dissociation of the 2/3 of cations completes the reaction. The reaction did not proceed completely, probably because of the trapping of monomers in the coordination network, a thermally reversible reaction associated with light absorption, and/or entropy contribution.[28] The low dissociation ratio of **1-FSA** (~30%) is attributed to reaction completing with the dissociation of one-third of cations (Figure 1b).[27]

Upon heating to 120°C, these photoproducts quantitatively reverted to their original ILs within 5 min, rendering the reaction fully reversible. The DSC investigation of the thermal reversible reaction of the photoproduct of **2-Tf$_2$N** showed a glass transition at 24°C and a broad endothermic peak at approximately 70°C ($\Delta H \approx 2$ kJ mol^{-1}) upon heating, which corresponded to thermal conversion from the coordination polymer to the original ILs. This finding suggests that this photoproduct exhibits a weaker network structure than the photoproduct of **3-FSA**, which shows an endothermic peak at approximately 80°C ($\Delta H = 5.2$ kJ mol^{-1}).[30] This observation is consistent with their dynamic viscoelasticity, as discussed below. **4-FSA** containing the NMe_2 substituent exhibited an extremely slow photoreaction, with only 30% dissociation of the cation after 3 h photoirradiation. This effect resulted from the high viscosity of **4-FSA** and strong electron-donating effect of the NMe_2 group, which stabilized the sandwich complex.

Reactivity of ILs with Coordinating Anions. Figure 5b (right) shows the cation dissociation ratios of ILs containing coordinating anions (**2-TfNCN**, **2-B(CN)$_4$**, and **2-BF$_2$(CN)$_2$**) against the photoirradiation time. Cation dissociations of 86%, 91%, and 75% were observed in

approximately 20, 30, and 15 min, respectively, and no further dissociation was observed with continued photoirradiation. Furthermore, their conversions were consistent with the dissociation ratios. These ILs exhibited faster reaction rates and higher conversions than ILs with noncoordinating anions (**2-FSA**: 70% in 30 min, **2-Tf_2N**: 75% in 80 min, see above), due to the strong coordination ability of the CN groups in the anion. The photoproduct of **2-TfNCN** decomposed within a minute in air, forming a blue viscous material (Figure S2a), but the others were stable in air.

The thermal reactivity of photoproducts varied with the anion. Heating the photoproduct of **2-TfNCN** at 120°C for 10 min caused a reverse reaction quantitatively. By contrast, the photoproduct of **2-$B(CN)_4$** underwent a two-step reversion (Figure 4c). Heating at 120°C transformed it into a yellow-orange viscoelastomer within 10 min, which was a solid–liquid mixture, as revealed in microscopic examination (Figure S3). The solid component was a crystalline coordination polymer, while the liquid component was a mixture of dissociated ligand and thermally-produced original IL (see below). Additionally, heating this mixture at 180°C for 10 min almost gave the original IL. In contrast to the other ILs, the photoreaction of **2-$BF_2(CN)_2$** was irreversible. The heating of the photoproduct of the IL at 120°C for 5 min resulted in its decomposition to yield a colorless solid, which was insoluble in common solvents (Figure S2b).

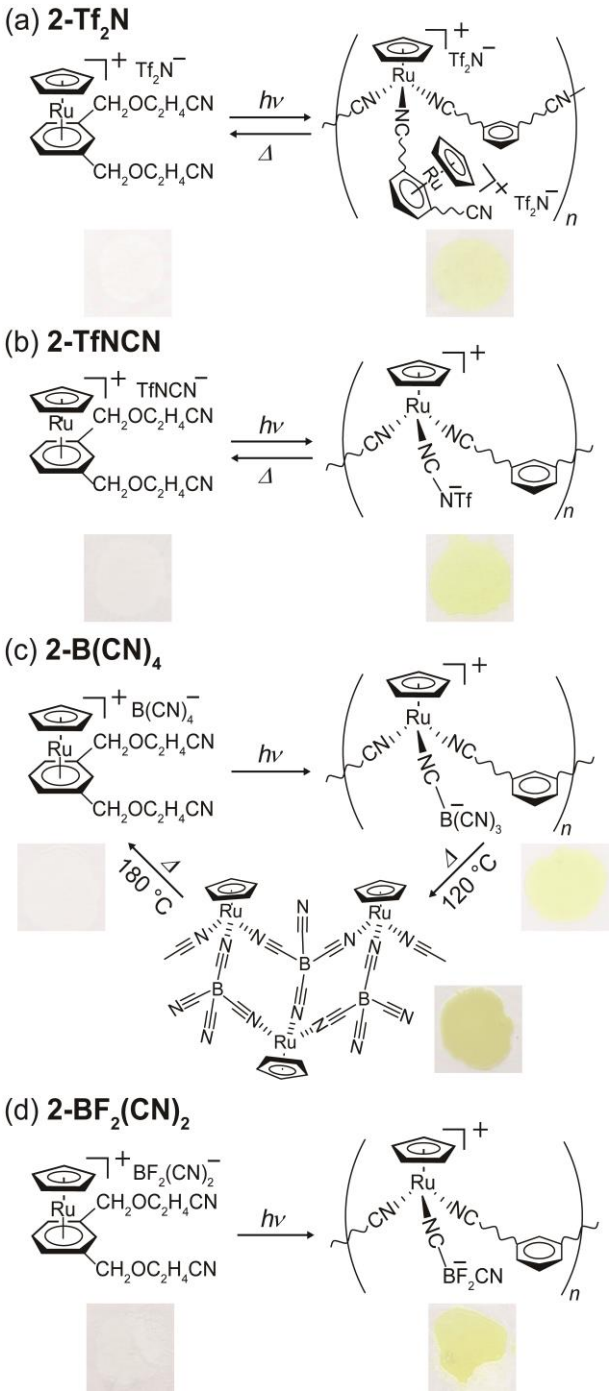

Figure 4. Reaction schemes of (a) **2-Tf$_2$N**, (b) **2-TfNCN**, (c) **2-B(CN)$_4$**, and (d) **2-BF$_2$(CN)$_2$**. Photographs of the ILs and photoproducts sandwiched between the quartz plates are shown below each structure.

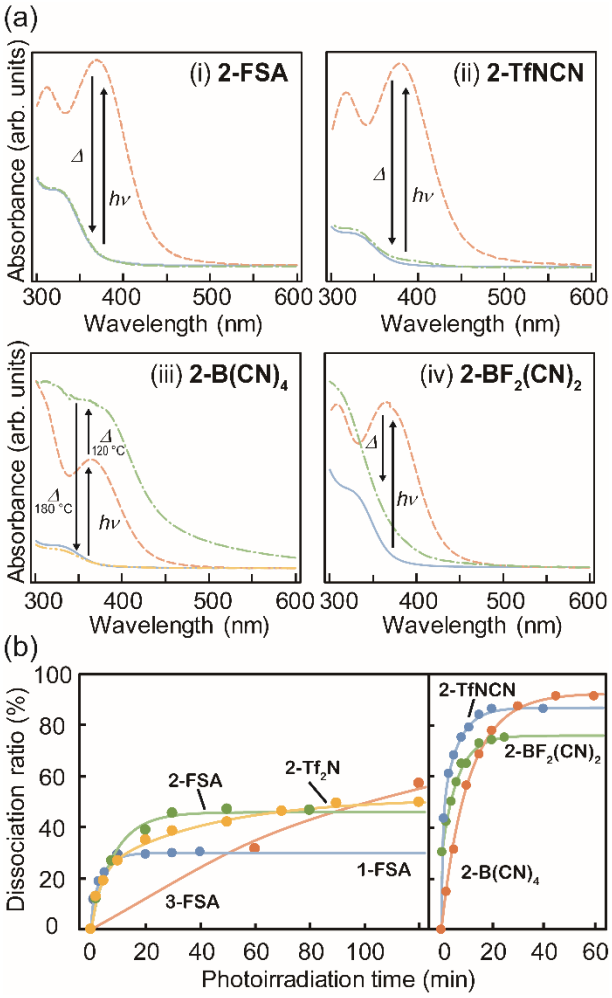

Figure 5. (a) UV–Vis spectra of each IL measured before photoirradiation, after UV photoirradiation, and after subsequent heating at 120°C. (b) Cation dissociation ratios vs. photoirradiation time for ILs with noncoordinating anions (**1-FSA**,[27] **2-FSA**, **2-Tf$_2$N**, and **3-FSA;**[27] left) and coordinating anions (**2-TfNCN**, **2-B(CN)$_4$**, and **2-BF$_2$(CN)$_2$**; right).

Table 2. Photoreaction time, dissociation ratio, conversion, and reversibility of photoreactions of the ILs

	Photoreaction time[b] (min)	Dissociation ratio[c] (%)	Conversion[d] (%)	Reversibility
2-FSA	~30	47	70	Y
2-Tf$_2$N	~80	50	75	Y

2-TfNCN	~20	86	86	Y (under N_2)
2-B(CN)$_4$	~30	91	91	Y (incomplete)
2-BF$_2$(CN)$_2$	~15	75	75	N
1-FSA [a]	~10	30	90	Y
3-FSA [a]	~300	82	82	Y
4-FSA		(30)[e]	(30)[e]	

[a]Ref. 27. [b]Time required for the photoreaction to saturate. [c]Cation photodissociation ratio. [d]Calculated from the dissociation ratio, considering the number of cyano groups. [e]Values after 180-min photoirradiation.

Spectroscopic Investigation. Structural changes in the ILs upon photoirradiation and heating were investigated using spectroscopic techniques. As seen in Figures 5a and S4, the UV–Vis spectra of each IL before photoirradiation were almost similar to that of $[CpRu(C_6H_6)]PF_6$ ($\varepsilon_{(320\ nm)}$ = 136 M^{-1} cm^{-1}, in acetonitrile[37]). After photoirradiation, each spectrum exhibited absorption peaks characteristic of cyano coordination at approximately 310 and 370 nm,[27] corresponding to a color change to yellow. Meanwhile, in the FT-IR spectra, peak shifts reflecting coordination structure changes[30] were observed upon photoirradiation (Figure S5). In **2-Tf$_2$N**, the CN stretching vibration shifted from 2251 to 2278 cm^{-1}, and the C=C stretching vibration shifted from 1501 and 1527 cm^{-1} to 1579 and 1603 cm^{-1} upon photoreaction. Similar shifts were observed for **2-FSA**. The anion CN stretching vibration peaks in **2-TfNCN**, **2-B(CN)$_4$**, and **2-BF$_2$(CN)$_2$** were observed at 2193, 2220, and 2208 cm^{-1}, respectively, and the ligand CN peaks were observed at approximately 2250 cm^{-1} for each IL. These peaks decreased after photoirradiation, and new anion CN stretching peaks emerged at 2240, 2230, and 2218 cm^{-1}, respectively, indicating anion coordination.

Heating the photoproducts of **2-FSA**, **2-Tf$_2$N**, and **2-TfNCN** at 120°C resulted in reversible reactions, restoring the original UV–Vis and FT-IR spectra. By contrast, heating the photoproduct

of **2-$BF_2(CN)_2$** resulted in decomposition; an intense absorption peak appeared below 400 nm in the UV–Vis spectrum (Figures 5a-iv), and the IR spectrum displayed a broad, strong peak at approximately 2100 cm^{-1}, which is probably ascribed to the corresponding anion decomposition product.

The spectra of the photoproduct of **2-$B(CN)_4$** reverted to their original spectrum in two steps, upon heating at 120°C and then at 180°C (Figure 4c). The photoproduct was a homogeneous viscoelastomer, which was probably an anion-coordinated coordination polymer bridged by arene ligands. Heating this material at 120°C for 10 min caused sudden darkening to yellow-orange, and a broad, stronger absorption peak appeared in the UV–Vis spectrum (Figure 5a-iii); furthermore, the CN stretching peak in the IR spectrum was blue-shifted (2235 cm^{-1}) compared with that of the photoproduct (2230 cm^{-1}). This change indicates the structural transformation to a more robust $B(CN)_4$-bridged coordination polymer,[38] releasing the bridging arene ligand. ^1H NMR spectrum of the product, which was a solid–liquid mixture, in acetonitrile revealed that 60% of cations transformed into the anion-bridged coordination polymer while the remaining 40% further transformed into the original IL. Washing with acetonitrile or dichloromethane removed the free ligand and IL, yielding a yellow coordination polymer insoluble in dichloromethane, and its plausible structure is shown in Figure 4c. The UV–Vis and FT-IR spectra of the solid coordination polymer were identical to those of the $B(CN)_4$-bridged amorphous coordination polymer[38] produced via the photoreaction of $[CpRu(PhR)]B(CN)_4$ (R = alkyl substituent), indicating their close similarity in local structures. In contrast to the amorphous solid, the current solid was crystalline (see below), probably because it is a thermodynamic product obtained after heating. Additionally, the subsequent heating of the mixture to 180°C for 10 min reverted the spectra to those of the original IL, but a small amount of unreacted coordination polymer remained owing to inhomogeneity, as visually and

spectroscopically observed.

PDF analysis. To understand structural changes induced by photoirradiation, X-ray PDF analysis was conducted on **2-Tf_2N** and **2-$B(CN)_4$**. Their PDF profiles are shown in Figures 6a and 6b, respectively, wherein correlation peaks observed at 2.2 Å and 1.5 Å can be assigned to Ru–C bonds and other intramolecular bonds such as C–C, respectively. The correlation peak at 1.5 Å is more pronounced for **2-Tf_2N** than for **2-$B(CN)_4$** because the former contains a larger number of S–E (E = O, N, or F) bonds in its anion. After photoirradiation, the PDF profiles of both samples show only slight changes, attributable to minor alterations in their bond lengths (e.g., Ru–C = 2.2 Å, Ru–N = 2.1 Å)[27] and moderate conversion.

In the plot of the structure factor $S(Q)$ of **2-$B(CN)_4$** (Figure S6), a slight shift in peaks to higher Q values is observed after photoirradiation, indicating the development of short-range order. This shift suggests that the transformation to a coordination polymer likely results in shorter Ru...Ru distances, leading to a more ordered network structure. However, such a change was not observed in **2-Tf_2N**.

Note that, after heating the photoproduct of **2-$B(CN)_4$** at 120°C, Bragg peaks appeared in the $S(Q)$ plot (Figure S6), indicating the transformation from an amorphous coordination polymer to a crystalline coordination polymer. In the PDF profile of the sample (Figure 6b), an increase in the peak intensity was observed at 5.5–6.0 and 7.5 Å after heating, which further supports the anion-bridged coordination polymer structure as they correspond to the Ru...Ru distances between adjacent CpRu units and distances bridged by the anion, respectively. These results support structural changes induced by photoirradiation and subsequent heating, as shown in Figure 4c.

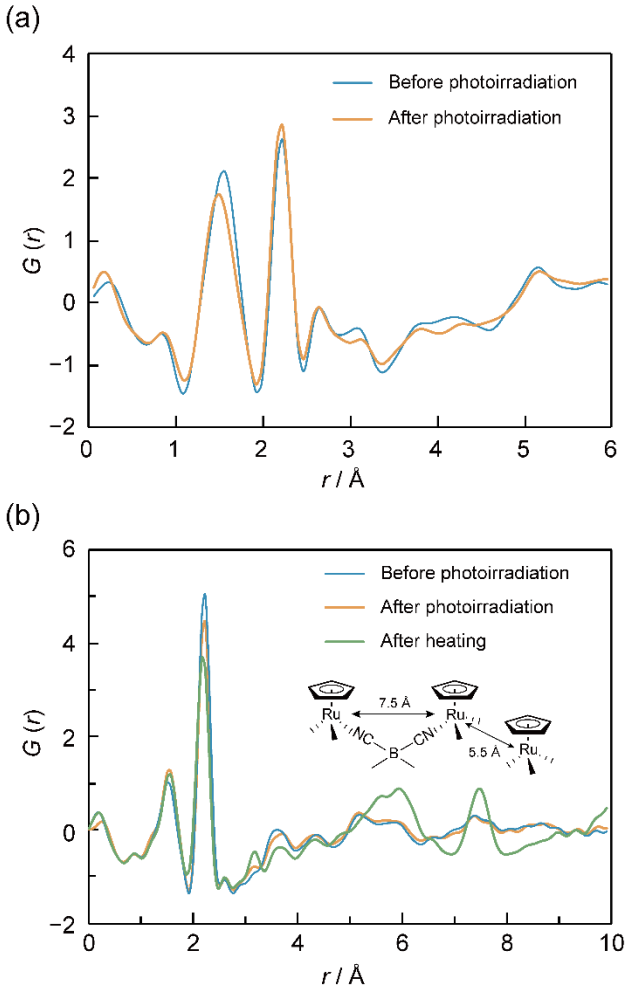

Figure 6. PDF profiles of (a) **1-Tf$_2$N** before and after photoirradiation and (b) **1-B(CN)$_4$** before and after photoirradiation and after subsequent heating at 120°C.

Ionic Conductivity Changes. The ionic conductivity of each IL studied was measured on a sample sandwiched between an interdigitated electrode and a quartz plate. Figure 7 shows ionic conductivity changes against the photoirradiation time for the ILs at 25°C. Photoirradiation reduced their ionic conductivity due to cation immobilization, and the observed conductivity changes were repeatable in most ILs under repeated cycles of photoirradiation and heating, exhibiting conductivity changes as large as that of **3-FSA** with much shorter response time.

The ionic conductivities of **2-FSA** and **2-Tf$_2$N** at 25°C were comparable at 1.7×10^{-4} and

1.6×10^{-4} S cm^{-1}, respectively, which decreased upon photoirradiation by approximately one and two orders of magnitude, respectively, to 0.76×10^{-5} and 1.3×10^{-6} S cm^{-1} (Figure 7a(i), Table 1). The longer response time observed in Figure 7a than in Figure 5b is attributed to different experimental setups. The larger ionic conductivity of the photoproduct of **2-FSA** is due to the greater mobility of its smaller anion, which is the primary carrier after photoreaction. **2-B(CN)$_4$** and **2-TfNCN** exhibited similar conductivity changes, while **2-BF$_2$(CN)$_2$** demonstrated a slightly larger change (Figure 7a(ii)). Figure 7b displays changes in the ionic conductivity of the ILs upon photoirradiation, in which **2-Tf$_2$N** and **2-TfNCN** showed a greater change than **3-FSA**, while **2-B(CN)$_4$** demonstrated a comparable change. The ionic conductivities of these ILs before and after photoirradiation were intermediate between those of **1-FSA** and **3-FSA**. **2-BF$_2$(CN)$_2$** exhibited a larger conductivity change but is not shown in the figure because the reaction was irreversible.

Furthermore, the conductivity changes under photoirradiation–heating (120°C) cycles were investigated (Figure 7c). **2-Tf$_2$N**, **2-FSA**, and **2-TfNCN** exhibited fully repeatable ionic conductivities, whereas repeatability was significantly reduced for **2-B(CN)$_4$** in each cycle because heating at 120°C is insufficient to complete the reverse reaction. **2-BF$_2$(CN)$_2$** underwent an irreversible change upon heating.

Figure 7d shows the temperature dependence of the ionic conductivities of **2-Tf$_2$N**, **2-TfNCN**, and **2-B(CN)$_4$** between 0°C and 120°C before and after photoirradiation. The photoproduct of **2-Tf$_2$N** displayed a linear trend up to approximately 85°C upon heating, after which an inflection point occurred owing to thermal reaction. Consistently, during heating above 110°C and subsequent cooling, the ionic conductivity remained the same as that before photoirradiation. **2-TfNCN** and its photoproduct exhibited similar results. The temperature dependence before and after photoreaction was analyzed using the Vogel–Fulcher–Tammann

(VFT) equation ($\sigma(T) = AT^{-1/2} \exp[-E_a/k_B(T-T_0)]$)[39] and the Arrhenius equation ($\sigma(T) = \sigma_\infty \exp(-E_a/k_BT)$), respectively, where A represents the number of carrier ions, E_a is the activation energy for ion transport, and T_0 is the ideal glass transition temperature. Table 3 contains the resulting fitting parameters. The value of A for **2-Tf$_2$N** (25 S K$^{1/2}$ cm^{-1}) was comparable to those of **1-FSA** (19 S K$^{1/2}$ cm^{-1}) and **3-FSA** (17 S K$^{1/2}$ cm^{-1}), whereas the smaller value obtained for **2-TfNCN** (11 S K$^{1/2}$ cm^{-1}) may be ascribed to its ion-pair formation tendency owing to the presence of the –NCN group in the anion. Similarly, the much smaller σ_∞ value for the photoproduct of **2-TfNCN** (~10^6 S cm^{-1}) than that of **2-Tf$_2$N** (~10^{12} S cm^{-1}) reflects the marked difference in their temperature dependence, probably resulted from anion coordination. Furthermore, **2-B(CN)$_4$** exhibited a similar temperature dependence, but its photoproduct transformed into a solid–liquid mixture at 120°C, which was the highest temperature that can be measured with the instrument, and did not fully revert to the original IL. Therefore, its ionic conductivity at 120°C did not match the value before photoirradiation, and the temperature dependence during subsequent cooling differed from that of the original IL. We found that **2-TfNCN** exhibited an irreversible electrode reaction at lower applied voltages than the other ILs, suggesting a smaller electrochemical window. This behavior probably results from its NCN-conjugated anion structure, which may also contribute to the air sensitivity of its photoproduct.

We previously found that Ru-containing ILs with higher viscosities tend to exhibit slower photoreaction rates compared to those with lower viscosities..[27-29] The ILs with two substituents investigated in the current study exhibited a much faster response than **3-FSA** while maintaining large conductivity changes. This feature, attributed to their lower viscosity, resulted from the molecular design with reduced number and length of cation substituents.

Table 3. Ionic conductivity of **2-Tf$_2$N** and **2-TfNCN** and parameters for their analysis

		$\sigma_{25°C}$ (S cm^{-1})	E_a (meV)	A (S K$^{1/2}$ cm^{-1}) [a]	T_0 (K) [a]	σ_∞ (S cm^{-1}) [b]
2-Tf$_2$N	Before irradiation	1.6×10^{-4}	98.5	25.4(14.8)	176.2(15)	—
	After 3 h irradiation	1.3×10^{-6}	1110	—	—	$3.44(0.6) \times 10^{12}$
2-TfNCN	Before irradiation	1.5×10^{-4}	84.7	11.1 (10.4)	186.7(12.9)	—
	After 2.5 h irradiation	1.0×10^{-6}	724	—	—	$1.37(0.3) \times 10^{6}$

[a]Parameters for the VFT equation. [b]Parameters for the Arrhenius equation.

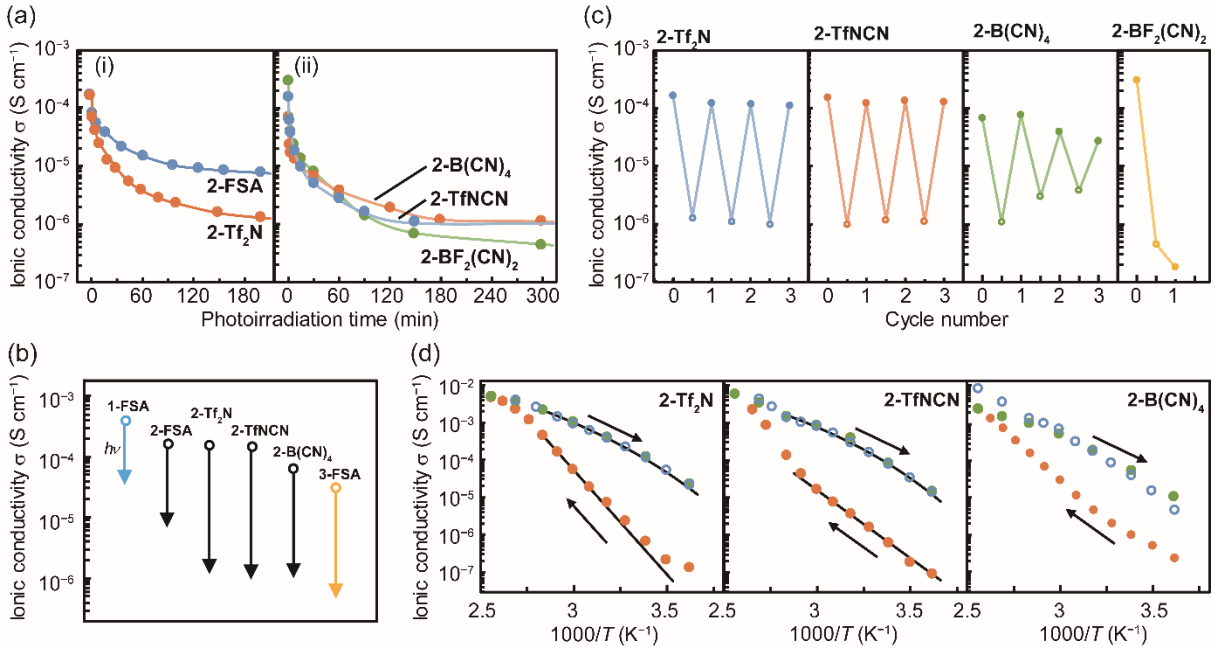

Figure 7. (a) Changes in the ionic conductivity of (i) **2-FSA** and **2-Tf$_2$N** and (ii) **2-TfNCN**, **2-B(CN)$_4$**, and **2-BF$_2$(CN)$_2$** at 25°C plotted against the photoirradiation time. (b) Changes in the ionic conductivity of each IL. Values before (○) and after (▼) photoirradiation. (c) Ionic conductivity of **2-Tf$_2$N**, **2-TfNCN**, **2-B(CN)$_4$**, and **2-BF$_2$(CN)$_2$** measured at 25°C during repeated cycles of photoirradiation (○) and 120°C heating (●). (d) Temperature dependence of the ionic conductivity of **2-Tf$_2$N**, **2-TfNCN**, and **2-B(CN)$_4$** before (○, cooling run) and after (●, heating and subsequent cooling) photoreactions. The temperature dependences before and after

photoirradiation are fitted by the VFT and Arrhenius equations, respectively (solid lines).

Viscoelasticity. The viscoelasticities of **2-FSA** and **2-Tf$_2$N** at 25°C were measured before and after photoirradiation to examine the effect of the number of cation substituents on the viscoelasticity. The photoproducts showed intermediate elastic moduli between those of **1-FSA** and **3-FSA**, which was consistent with the dimensionality of the network structures in the photoproducts.

The viscosities of **2-FSA** and **2-Tf$_2$N** were 1.00 and 1.87 Pa·s, respectively (Table 1), while their complex viscosities after photoirradiation at an angular frequency of 10 rad s^{-1} (0.1% strain) were comparable at 1542 and 1566 Pa·s, respectively. These values were intermediate between those of the photoproducts of **1-FSA** (5.2 Pa·s) and **3-FSA** (>10^5 Pa·s).

Figure 8 shows the complex moduli of these ILs after photoirradiation (0.1% strain). The photoproduct of **2-FSA** exhibited elastic behavior (tan $\delta = G''/G' < 1$), with the storage modulus (G') exceeding the loss modulus (G'') below approximately 4 rad s^{-1}, whereas G'' exceeded G' above this frequency, exhibiting viscous behavior (tan $\delta > 1$). The photoproduct of **2-Tf$_2$N** displayed elastic behavior up to a higher angular frequency of ~40 rad s^{-1}, indicating that the photoproducts of **2-FSA** and **2-Tf$_2$N** were in the rubber and glass–rubber transition regions, respectively, which is consistent with the latter's higher T_g. The strain-dependent elastic modulus revealed that the photoproduct of **2-Tf$_2$N** presented a decrease in storage modulus at larger strain than the photoproduct of **2-FSA** (Figure S7), which was indicative of its stronger network structure. These photoproducts were viscoelastic with one order of magnitude smaller storage moduli (~10^4 Pa) than the photoproduct of **3-FSA** (~10^5 Pa), exhibiting a greater angular frequency dependence for the loss modulus.

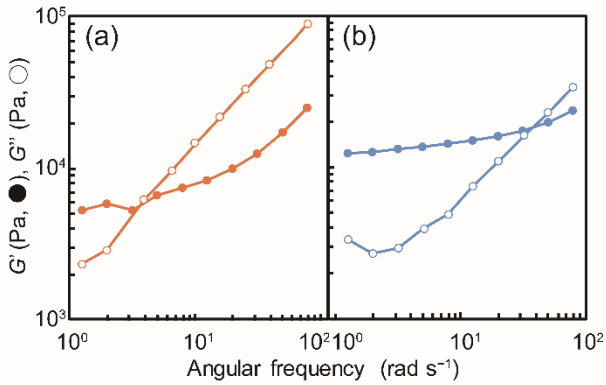

Figure 8. Storage modulus *G*' (●) and loss modulus *G*'' (▲) of the photoproducts of (a) **2-FSA** and (b) **2-Tf$_2$N** at 25°C (strain 0.1%).

CONCLUSIONS

Advancing our continuous research on stimuli-responsive ILs, we investigated the photoreactivity and physical properties of Ru-containing ILs with two coordinating substituents in the cation. Upon UV photoirradiation, these ILs underwent transformation into viscoelastic coordination polymers, which mostly underwent a reversible reaction upon heating, reverting to their original ILs. Coordinating anion salts exhibited higher conversions and faster photoreaction rates than noncoordinating anion salts. The developed ILs exhibited much faster responses than previously reported ILs with three cyanoalkyl substituents and presented similar or even greater ionic conductivity changes. These enhanced photoreactivity and property changes resulted from the molecular design using fewer and shorter substituents in the cation, which led to lower viscosity. These findings provide insights into the development of stimuli-responsive electronic devices, such as stimuli-tunable capacitors using ILs. Employing ILs in device application is advantageous owing to the minimal amount required for operation. Further development of photoreactive ILs exhibiting structural changes and additional functions is underway in our laboratory.

Supporting Information

The Supporting Information is available free of charge at https://pubs.acs.org/doi/

^{1}H NMR spectra, photographs, and FT-IR spectra of the ILs, UV–Vis spectra of **2-Tf_2N**, dynamic viscoelasticity data for **2-FSA** and **2-Tf_2N**, and PDF data for **1-$B(CN)_4$** (PDF)

ACKNOWLEDGMENTS

We thank Prof. Ryo Horikoshi (Osaka Sangyo University) for aiding us in instrumental analysis. Synchrotron experiments were performed in SPring-8 with the approval of the committee (Proposal No. 2023B2431).

Author Information

Corresponding Author

Tomoyuki Mochida - *Department of Chemistry, Graduate School of Science, Kobe University, 1-1 Rokkodai, Nada, Kobe, Hyogo 657-8501, Japan; Research Center for Membrane and Film Technology, Kobe University, 1-1 Rokkodai, Nada, Kobe, Hyogo 657-8501, Japan;*

https://orcid.org/0000-0002-3446-2145; Email: tmochida@platinum.kobe-u.ac.jp

Authors

Masato Shimada, Ryota Inoue, Ryo Sumitani - *Department of Chemistry, Graduate School of Science, Kobe University, 1-1 Rokkodai, Nada, Kobe, Hyogo 657-8501, Japan*

Yusuke Funasako - *Department of Applied Chemistry and Biochemistry, National Institute of Technology, Wakayama College, 77 Noshima, Nada, Gobo, Wakayama, Japan*

Hiroki Yamada - *Japan Synchrotron Radiation Research Institute (JASRI), Kouto 1-1-1, Sayo-cho, Sayo-gun, Hyogo 679-5198, Japan*

Author Contributions

The manuscript was written through contributions of all authors. All authors have given approval to the final version of the manuscript.

Funding Sources

This work was financially supported by the JSPS KAKENHI Grant-in-Aid for Transformative Research Areas (A) “Supra-ceramics” (grant numbers JP23H04629 (T.M.) and JP23H04642 (H.Y.)) and JSPS

KAKENHI (grant number JP20H02756).

Notes

The authors declare no competing financial interest.

REFERENCES

1. Baeg, K. J.; Binda, M.; Natali, D.; Caironi, M.; Noh, Y. Y. Organic Light Detectors : Photodiodes and Phototransistors. *Adv. Mater.* **2013**, 25, 4267–4295, DOI: 10.1002/adma.201204979

2. Wang, H.; Kim, D. H. Perovskite-based photodetectors: materials and devices. *Chem. Soc. Rev.* **2017**, *46*, 5204–5236, DOI: 10.1039/c6cs00896h

3. Zhang, J.; Zou, Q.; Tian, H. Photochromic Materials : More Than Meets The Eye. *Adv. Mater.* **2013**, *25*, 378–399, DOI: 10.1002/adma.201201521

4. Rice, A. M.; Martin, C. R.; Galitskiy, V. A.; Berseneva, A. A.; Leith, G. A.; Shustova, N. B. Photophysics modulation in photoswitchable metal-organic frameworks. *Chem. Rev*. **2020**, *120*, 8790–8813, DOI: 10.1021/acs.chemrev.9b00350

5. Santhosh, B. S.; Nakanishi, T. Nonvolatile functional molecular liquids. *Chem. Commun.* **2013**, *49*, 9373–9382, DOI: 10.1039/c3cc45192e

6. Cui, J.; Li, Yi, Chen, D.; Zhan, T. G.; Zhang, K. D. Ionic Liquid-Based Stimuli-Responsive Functional Materials. *Adv. Funct. Mater.* **2020**, *30*, 2005522, DOI: 10.1002/adfm.202005522

7. Xu, Y.; Chen, L.; Chen, J.; Chang, X.; Zhu, Y. Flexible and Transparent Pressure/Temperature Sensors Based on Ionogels with Bioinspired Interlocked Microstructures. *ACS Appl. Mater. Interfaces* **2022**, *14*, 2122–2131, DOI: 10.1021/acsami.1c22428

8. Chen, Z.; Gui, Q.; Wang, Y. Dynamic chemistry in ionic liquid-based conductor. *Green Chemical Engineering* **2021**, 2, 346–358, DOI: 10.1016/j.gce.2021.07.011

9. Pei, Y.; Zhang, Y.; Ma, J.; Fan, M.; Zhang, S.; Wang, J. Ionic liquids for advanced materials. *Materials Today Nano* **2022**, 100159, DOI: 10.1016/j.mtnano.2021.100159

10. Kaur, G.; Kumar, H.; Singla, M. Diverse applications of ionic liquids: A comprehensive review. *J. Mol. Liq.* **2022**, *351*, No 118556, DOI: 10.1016/j.molliq.2022.118556

11. Watanabe, M.; Thomas, M. L.; Zhang, S.; Ueno, K.; Yasuda, T.; Dokko, K. Application of Ionic Liquids to Energy Storage and Conversion Materials and Devices. *Chem. Rev.* **2017**, *117*, 7190–7239, DOI: 10.1021/acs.chemrev.6b00504

12. Tiago, G. A. O.; Matias, I. A. S.; Ribeiro, A. P. C.; Martins, L. M. D. R. S. Application of Ionic Liquids in Electrochemistry—Recent Advances. *Molecules* **2020**, *25*, 5812–5838, DOI: 10.3390/molecules25245812

13. Galinski, M.; Lewandowski, A.; Stepniak, I. Ionic liquids as electrolytes. *Chem. Rev.* **2006**, *51*, 5567–5580, DOI: 10.1016/j.electacta.2006.03.016

14. Matsuo, T.; Sato, D.; Koh, S. G.; Shima, H.; Naitoh, Y.; Akinaga, H.; Itoh, T.; Nokami, T.; Kobayashi, M.; Kinoshita, K. Dynamic Nonlinear Behavior of Ionic Liquid-Based Reservoir Computing Devices. *ACS Appl. Mater. Interfaces* **2022**, *14*, 36890–36901, DOI: 10.1021/acsami.2c04167

15. Sato, H.; Shima, H.; Nokami, T.; Itoh, T.; Honma, Y.; Naitoh, Y.; Akinaga, H.; Kinoshita, K. Memristors with Controllable Data Volatility by Loading Metal Ion-Added Ionic Liquids. *Front. Nanotechnol*. **2021**, *3*, No. 660563, DOI: 10.3389/fnano.2021.660563

16. Kuroda, K.; Shimada, Y.; Takahashi, K. CO_2-triggered fine tuning of electrical conductivity via tug-of-war between ions. *New J. Chem.* **2018**, *42*, 15528–15532, DOI: 10.1039/c8nj02642d

17. Hussan, K. P. S.; Moidu, H. H.; Thayyil, M. S.; Jinitha, T. V.; Antony, A.; Govindaraj, G. Physisorption mechanism in a novel ionogel membrane based CO_2 gas sensor. *J. Mater. Sci. : Mater. Electron.* **2021**, *32*, 25164–25174, DOI: 10.1007/s10854-021-06973-5

18. Zhang, J.; Xu, D.; Guo, J.; Sun, Z.; Qian, W.; Zhang, Y.; Yan, F. CO_2 Responsive Imidazolium-Type Poly(Ionic Liquid) Gels. *Macromol. Rapid Commun.* **2016**, *37*, 1194–1199, DOI: 10.1002/marc.201600069

19. Fernandes, L. C.; Pereira, N.; Tubio, C. R.; Lanceros, M. S. Highly Sensitive Humidity Sensor Based on Ionic Liquid−Polymer Composites. *ACS Appl. Polym. Mater.* **2019**, *1*, 2723–2730, DOI: 10.1021/acsapm.9b00675

20. Xiao, S.; Nie, J.; Tan, R.; Duan, X.; Ma, J.; Li, Q.; Wang, T. Fast-response ionogel humidity sensor for real-time monitoring of breathing rate. *Mater. Chem. Front.* **2019**, *3*, 484–491, DOI: 10.1039/c8qm00596f

21. Xie, Z. L.; Huang, X.; Taubert, A. DyeIonogels: Proton-Responsive Ionogels Based on a Dye-Ionic Liquid Exhibiting Reversible Color Change. *Adv. Funct. Mater.* **2014**, *24*, 2837–2843, DOI: 10.1002/adfm.201303016

22. Zhang, S.; Liu, S.; Zhang, Q.; Deng, Y. Solvent-dependent photoresponsive conductivity of azobenzene-appended ionic liquids. *Chem. Commun.* **2011**, *47*, 6641–6643, DOI: 10.1039/c1cc11924a

23. Wang, H.; Zhu, C. N., Zeng, H.; Ji, X.; Xie, T.; Yan, X.; Wu, Z. L.; Huang, F. Reversible Ion-Conducting Switch in a Novel Single-Ion Supramolecular Hydrogel Enabled by Photoresponsive Host–Guest Molecular Recognition. *Adv. Mater*. **2019**, 31, 1807328, DOI: 10.1002/adma.201807328

24. Ishida, K.; Morikawa, M.; Chikara, C.; Yamada, T.; Iwase, K.; Kawasaki, M.; Kimizuka, N. Photoliquefiable Ionic Crystals: A Phase Crossover Approach for Photon Energy Storage Materials with Functional Multiplicity. *Angew. Chem. Int. Ed.* **2015**, *54*, 1532–1536, DOI: 10.1002/anie.201410184

25. Nie, H.; Schauser, N. S.; Dolinski, N. D.; Hu, J.; Hawker, C. J.; Segalman, R. A.; Read de Alaniz, J. Light-controllable Ionic Conductivity in a Polymeric Ionic Liquid. *Angew. Chem. Int. Ed.* **2020**, *59*, 5123–5128, DOI: 10.1002/anie.201912921

26. Mochida, T. Organometallic Ionic Liquids Containing Sandwich Complexes: Molecular Design, Physical Properties, and Chemical Reactivities. *Chem. Rec.* **2023**, *23*, e202300041, DOI: 10.1002/tcr.202300041

27. Sumitani, R.; Yoshikawa, H.; Mochida, T. Reversible control of ionic conductivity and viscoelasticity of organometallic ionic liquids by application of light and heat. *Chem. Commun.* **2020**, *56*, 6189–6192, DOI: 10.1039/d0cc02786c

28. Mochida, T.; Sumitani, R. Reversible Formation of Soft Coordination Polymers from Liquid Mixtures of Photoreactive Organometallic Ionic Liquid and Bridging Molecules. *Soft Matter* **2020**, *16*, 9946–9954. DOI: 10.1039/D0SM01567A

29. Mochida, T.; Shimada, M.; Sumitani, R. Substituent effects on the photoreactivity of Ru-containing ionic liquids exhibiting reversible ionic conductivity changes. *J. Mol. Liq.* **2023**, *381*, 121822, DOI: 10.1016/j.molliq.2023.121822

30. Funasako, Y.; Mori, S.; Mochida, T. Reversible transformation between ILs and coordination polymers by application of light and heat. *Chem. Commun.* **2016**, *52*, 6277–6279, DOI: 10.1039/c6cc02807a

31. Shaplov, A. S.; Lozinskaya, E. I.; Vlasov, P. S.; Morozova, S. M.; Antonov, D. Y.; Aubert, P. H.; Armand, M.; Vygodskii, Y. S. New family of highly conductive and low viscous ionic liquids with asymmetric 2,2,2-trifluoromethylsulfonyl-N-cyanoamide anion. *Electrochim. Acta* **2015**, *175*, 254–260, DOI: 10.1016/j.electacta.2015.02.228

32. Bernhardt, E; Finze, M.; Willner, H. Eine effiziente Synthese von Tetracyanoboraten durch Sinterprozesse. *Z. Anorg. Allg. Chem.* **2003**, *629*, 1229–1234, DOI: 10.1002/zaac.200300047

33. Chaudhuri, S.; Verderame, M.; Mako, T. L.; Nuwan, Y. M.; Bandara, D. Y.; Fernando, A. I.; Levine, M. Synthetic β-Cyclodextrin Dimers for Squaraine Binding: Effect of Host Architecture on Photophysical Properties, Aggregate Formation and Chemical Reactivity. *Eur. J. Org. Chem.* **2018**, *17*, 1964–1974, DOI: 10.1002/ejoc.201800283

34. Yamada, H.; Nakada, K.; Takemoto, M.; Ohara, K. Fully Automated Measurement System for Temperature-Dependent X-Ray Total Scattering at Beamline BL04B2 at SPring-8. *J. Synchrotron Radiat.* **2022**, *29*, 549–554, https://doi.org/10.1107/S1600577521013527

35. Turnbull, D.; Cohen, M. H. In *Modern Aspects of the Vitreous State*; Mackenzie, J. D., Ed.; Butterworths, London, **1960**; Vol. I, pp. 38.

36. Wang, L. M.; Angel, C. A.; Richert, R. Fragility and thermodynamics in nonpolymeric glass-forming liquids. *J. Chem. Phys.* **2006**, *125*, 074505, DOI: 10.1063/1.2244551

37. Gill, T. P.; Mann, K. R. Photochemical properties of the cyclopentadienyl(η6-benzene)ruthenium(II) cation. The synthesis and reactions of a synthetically useful intermediate: the cyclopentadienyltris(acetonitrile)ruthenium(II) cation. *Organometallics* **1982**, *1*, 485–488, DOI: 10.1021/om00063a014

38. Ueda, T.; Tominaga, T.; Mochida, T.; Takahashi, K.; Kimura, S. Photogeneration of Microporous Amorphous Coordination Polymersfrom Organometallic Ionic Liquids. *Chem. Eur. J.* **2018**, *24*, 9490–9493, DOI: 10.1002/chem.201801365

39. Vila, J.; Gines, P.; Pico, J. M.; Franjo, C.; Jimenez, E.; Varela, L. M.; Cabeza, O. Temperature dependence of the electrical conductivity in EMIM-based ionic liquids Evidence of Vogel–Tamman–Fulcher behavior. Fluid Phase Equilib. **2006**, *242*,141–146, DOI: 10.1016/j.fluid.2006.01.022

Supporting Information

Controlling Ionic Conductivity in Organometallic Ionic Liquids through Light-Induced Coordination Polymer Formation and Thermal Reversion

Tomoyuki Mochida,*[a,b] Masato Shimada,[a] Ryota Inoue,[a] Ryo Sumitani,[a] Yusuke Funasako,[c] Hiroki Yamada[d]

[a]Department of Chemistry, Graduate School of Science, Kobe University, Rokkodai, Nada, Kobe, Hyogo 657-8501, Japan. E-mail: tmochida@platinum.kobe-u.ac.jp

[b]Research Center for Membrane and Film Technology, Kobe University, Rokkodai, Nada, Kobe, Hyogo 657-8501, Japan

[c]Department of Applied Chemistry and Biochemistry, National Institute of Technology, Wakayama College, 77 Noshima, Nada, Gobo, Wakayama, Japan

[d]Japan Synchrotron Radiation Research Institute (JASRI), Kouto 1-1-1, Sayo-cho, Sayo-gun, Hyogo 679-5198, Japan

Contents

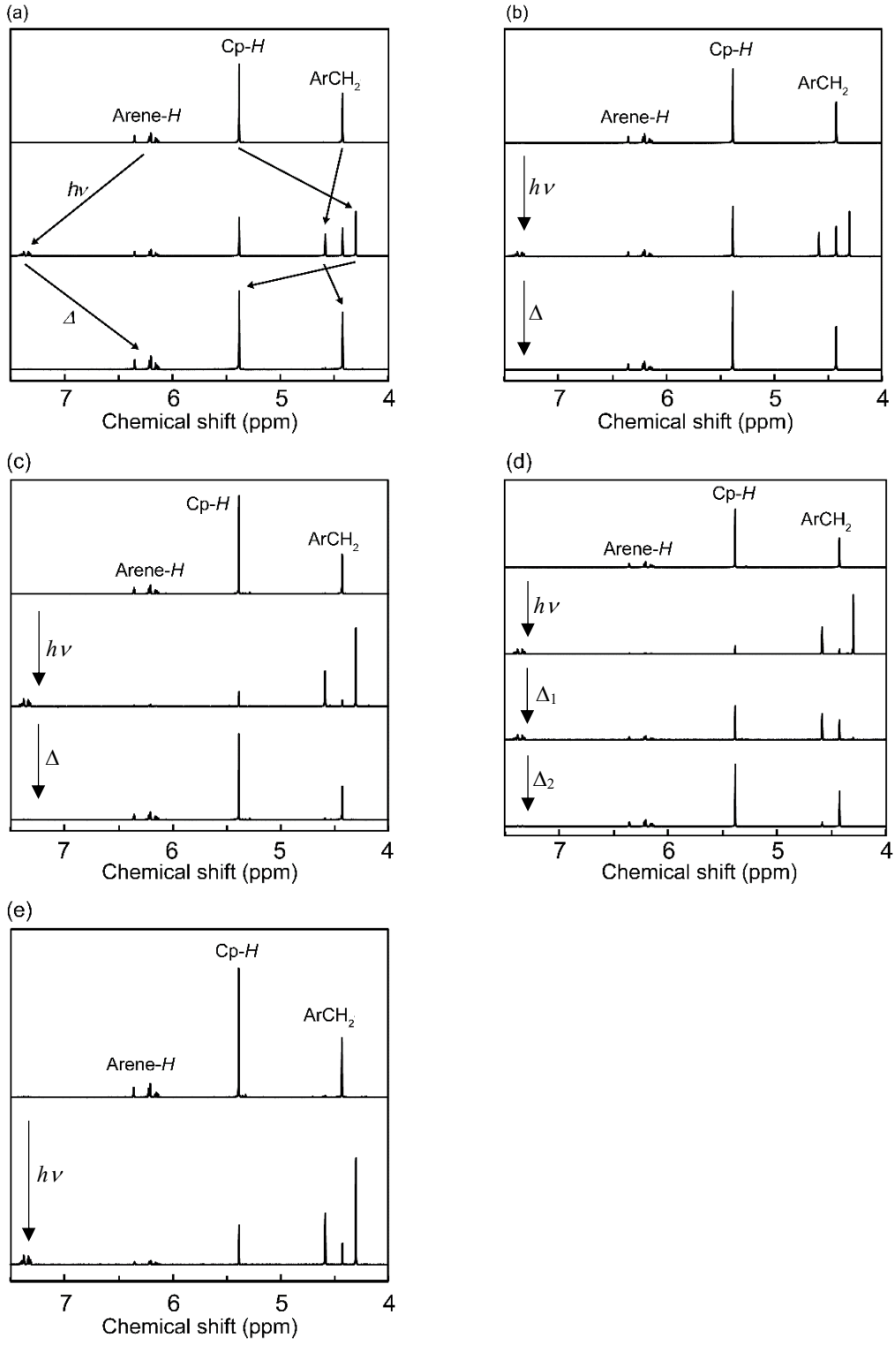

Figure S1. ^{1}H NMR spectra of (a) **2-Tf$_2$N**, (b) **2-FSA**, (c) **1-TfNCN**, (d) **2-B(CN)$_4$**, and (e) **2-BF$_2$(CN)$_2$** in CD_3CN measured before photoirradiation, after photoirradiation, and after subsequent heating at 120°C. In (e), the spectrum after heating is not shown because decomposition occurred. In (d), the spectrum after

subsequent heating at 180°C is also shown (bottom), and only the peaks of dissociated ligand and unreacted sandwich complexes were observed after heating at 120°C and 180°C because the dominant products were insoluble in the solvent.

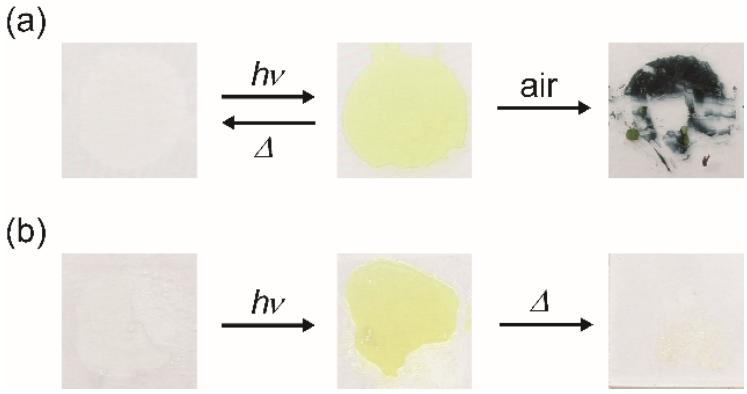

Figure S2. (a) Photographs of **2-TfNCN** before photoirradiation, after photoirradiation, and after exposure to air. (b) Photographs of **2-$BF_2(CN)_2$** before photoirradiation, after photoirradiation, and after heating at 120°C.

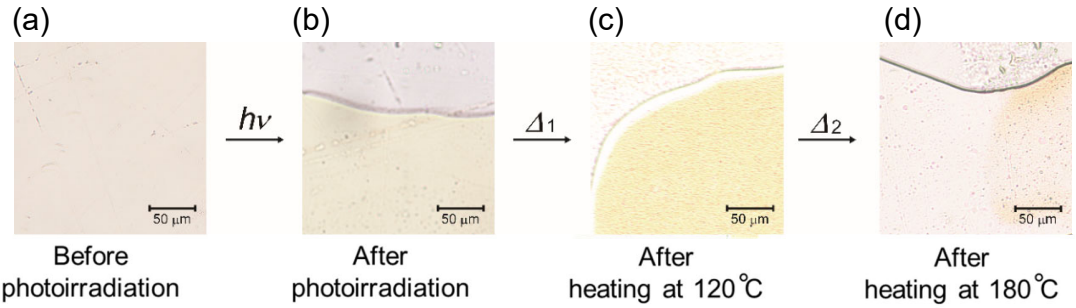

Figure S3. Microscopic photographs of **2-$B(CN)_4$** (a) before photoirradiation, (b) after photoirradiation, and subsequent heating (c) at 120°C and (d) at 180°C. The sample was sandwiched between quartz plates, but the quartz plate cover was removed in Figure (c).

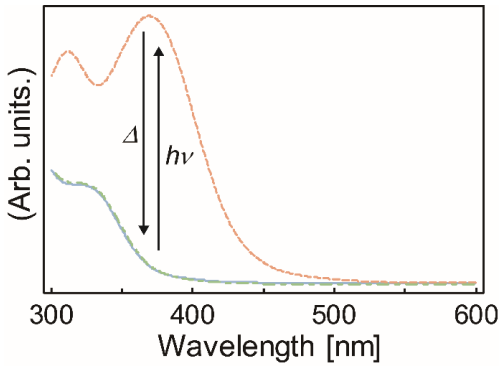

Figure S4. UV–Vis spectra of **2-Tf$_2$N** measured (a) before photoirradiation, (b) after 50 min photoirradiation, (c) and after subsequent 120°C heating for 5 min.

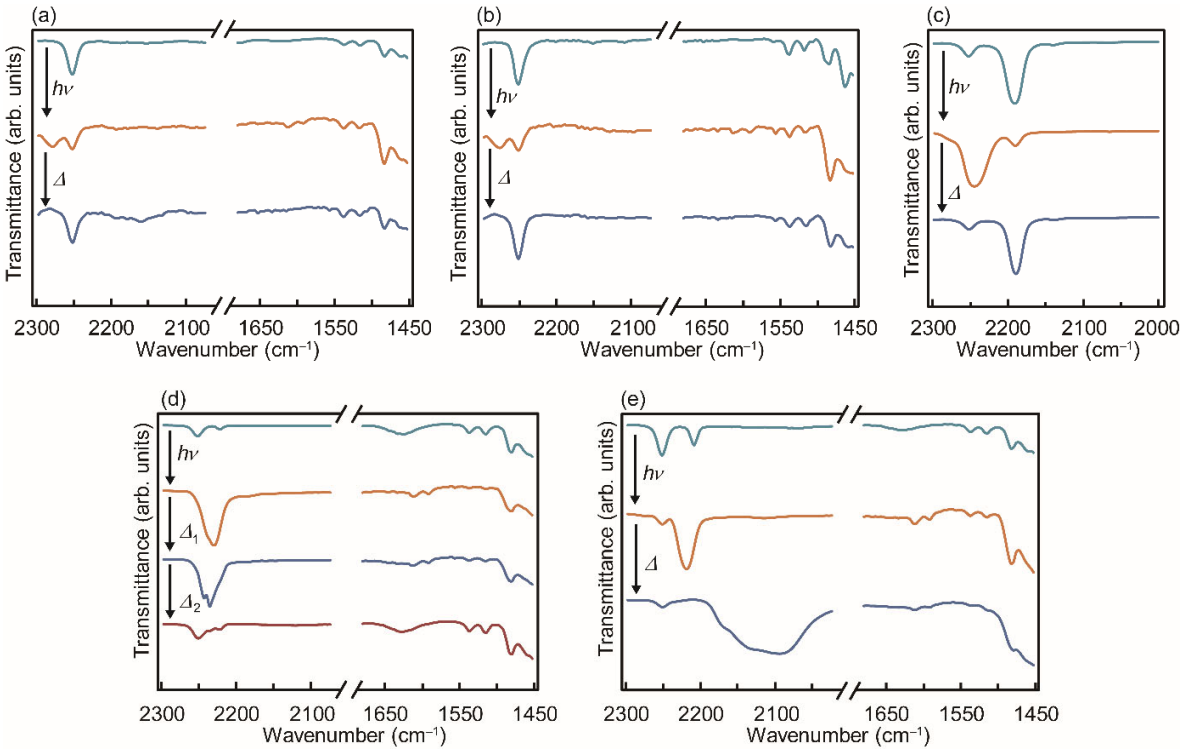

Figure S5. FT–IR spectra of (a) **2-Tf$_2$N**, (b) **2-FSA**, (c) **1-TfNCN**, (d) **2-B(CN)$_4$**, and (e) **2-BF$_2$(CN)$_2$** measured before photoirradiation, after photoirradiation, and after subsequent heating at 120°C. The spectrum after 180°C heating is shown in (d).

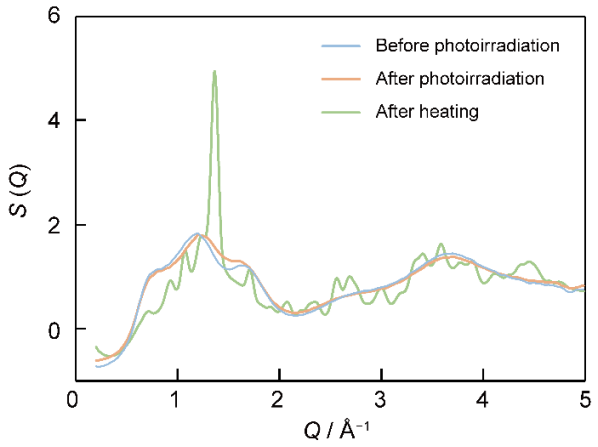

Figure S6. Plot of $S(Q)$ of **1-B(CN)$_4$** before and after photoirradiation, and after subsequent heating at 120 °C.

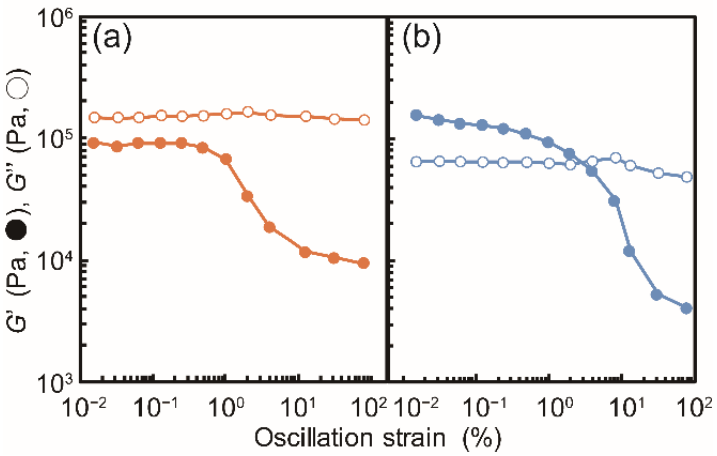

Figure S7. Strain dependence of the storage moduli G' (●) and loss moduli G'' (○) of the photoproducts of (a) **2-FSA** and (b) **2-Tf$_2$N** (25°C, angular frequency 10 rad s^{-1}).